Biosensors and Bioelectronics 195 (2022) 113658

Contents lists available at ScienceDirect

Biosensors and Bioelectronics

journal homepage: www.elsevier.com/locate/bios

Shaped DNA origami carrier nanopore translocation influenced by aptamer based surface modification

Taoli Ding [a], Jing Yang [b,1], Juan Wang [b,c], Victor Pan [d], Zuhong Lu [f,**], Yonggang Ke [d,e,***], Cheng Zhang [a,*]

[a] Key Lab of High Confidence Software Technologies, Department of Computer Science and Technology, School of Electronics Engineering and Computer Science, Peking University, Beijing, 100871, China
[b] School of Control and Computer Engineering, North China Electric Power University, Beijing, 102206, China
[c] Bio-evidence Sciences Academy, Xi'an Jiaotong University, Xi'an, Shaanxi, 710049, China
[d] Wallace H. Coulter Department of Biomedical Engineering, Georgia Institute of Technology and Emory University, Emory University School of Medicine, Atlanta, GA 30322, United States
[e] Department of Chemistry, Emory University, Atlanta, GA 30322, United States
[f] The State Key Laboratory of Bioelectronics, Southeast University, Nanjing, China, 211189

ARTICLE INFO

Keywords:
Solid state nanopore
DNA origami
Surface modification
Aptamer/target binding
Single molecular detection

ABSTRACT

DNA origami is widely used as a translocation carrier to assist solid-state nanopore analysis, e.g., soft linear origami carrier and special-shaped origami structures. In the linear origami carriers based nanopore sensing, molecular modifications induced tiny structural and charge changes, can result in significant variations on translocation signals to facilitating single-molecule sensing. However, an understanding on the influences of surface modifications on special-shaped DNA origami structures during solid-state (SS) nanopores translocation is still far elusive. Herein, we reported a surface modification strategy using aptamer/target-binding to influence the translocation of the shaped origami ribbon carrier through SS-nanopore. Our measurements indicate that the translocation signal variations can respond to ATP/aptamer binding on the carrier surface, even to the surface modifications induced by spatial distributions and enzyme catalysis. Meanwhile, the results also suggest a possibility to identify small spatial and electronic changes on DNA origami by using SS-nanopore. We envision that the surface aptamer-binding influenced origami translocation strategy could find more applications in origami carrier assisted SS-nanopore sensing and detection.

1. Introduction

Detecting the conductivity change across a nanopore is a highly sensitive and label-free single molecular technique for analyzing biomolecules (Plesa et al., 2016; Wei et al., 2012; Alibakhshi et al., 2017; Doroschak et al., 2020; Shasha et al., 2014; Carlsen et al., 2014a,b; Li et al., 2020; Mcmullen et al., 2014; Tourancheau et al., 2021; Sun et al., 2019). Nanopore detection has been used for a large variety of sensing applications, including small molecule sensing (Lin et al., 2017; Rivas et al., 2018; Spruijt et al., 2018; Zhang et al., 2021; Langecker et al., 2012; Bulushev et al., 2016), nucleic acids sequencing (Kovaka et al., 2020; Giesselmann et al., 2019; Rand et al., 2017), molecular structural change detections (Zahid et al., 2016; Plesa et al., 2014; Raveendran et al., 2020; Guo et al., 2018) and studies of molecular interactions (Kwak et al., 2016; Shim et al., 2015; Kawano et al., 2011). However small biomolecules (e.g. proteins and DNA) pass through solid-state (SS) nanopores in a random order, which makes the translocation signal unable to tell the spatial organization of the target (Alibakhshi et al., 2017; Rivas et al., 2018; Kwak et al., 2016). One-dimensional linear DNA origami carrier assisted nanopore detections have been recently developed to escort targets through the SS-nanopore (Bell et al., 2015; Plesa et al., 2015a,b; Kong et al., 2016; Chen et al., 2019). The ductile

* Corresponding author. Key Lab of High Confidence Software Technologies, Department of Computer Science and Technology, School of Electronics Engineering and Computer Science, Peking University, Beijing, 100871, China.
** Corresponding author. The State Key Laboratory of Bioelectronics, Southeast University, Nanjing, China, 211189.
*** Corresponding author. Department of Chemistry, Emory University, Atlanta, GA, 30322, United States.
E-mail addresses: zhlu@seu.edu.cn (Z. Lu), yonggang.ke@emory.edu (Y. Ke), zhangcheng369@pku.edu.cn (C. Zhang).
[1] The author contributed equally to the first author.

https://doi.org/10.1016/j.bios.2021.113658
Received 16 June 2021; Received in revised form 16 September 2021; Accepted 18 September 2021
Available online 27 September 2021

linear carrier enables simple control of the number and one-dimensional ordered arrangement of the target binding. During the linear carriers based nanopore sensing, molecular-binding modifications induced tiny structural and charge changes, can result in significant variations on translocation signals to facilitating single-molecule sensing (Bell et al., 2015, 2016; Yu et al., 2015). Recently, the linear carrier modifications based nanopore strategy has been widely used to detect proteins with the differences on their structures and electric charges (Bell et al., 2015; Kong et al., 2016), to investigate DNA conformations (Plesa et al., 2016; Kowalczyk et al., 2010), to encode digital information (Bell et al., 2016), and to determine dsDNA translocation velocity (Plesa et al., 2014).

Inspired by the one-dimensional linear DNA carrier, a special-shaped DNA origami with well-defined size and rigid shape, provide a designable and accurate spatial control for target molecules to translocate through SS-nanopore. For example, it is recently reported by Keyser's group that passing of a shaped DNA origami bundle can be influenced by introducing neutral polymers (Wang et al., 2019). The knowledge about the nanopore translocation of the shaped origami will greatly contribute to the potential applications of the various programable origami structures in nanopore sensing. However, an understanding on the influences of surface modifications on special-shaped DNA origami during SS-nanopores translocation is still far elusive. Meanwhile, it is still difficult to effectively influence the origami translocation process by the surface modification strategy, due to the rather rigid origami structures and much higher molecular weights.

In this work, we reported the SS-nanopore translocations of the shaped origami ribbon were influenced by a surface modification strategy based on aptamer/target binding (Fig. S17,18 and 19). Briefly, ATP-binding aptamers were designed at specific locations on the surface of the origami ribbon carrier. The binding of ATP with aptamer can induce structural and electronic charge changes on the origami carrier surface, thus influencing the nanopore translocation process and corresponding signal variations. In the experiments, the origami nanopore translocations were regulated by controls of different surface modifications, including ATP/aptamer binding, modification spatial distributions and enzymatic digestion.

2. Material and methods

2.1. Design and assembly of DNA origami structures

The DNA origami ribbon was designed by using Tiamat software. The details of the DNA origami structure assembly could be found in the support information (Fig. S3, S4 and S5). The assembly of the DNA carriers were achieved by mixing 221 32-mer staple DNA strands with single-stranded M13mp18 DNA strand in a one-pot reaction (the staple DNA strands (Table S3) were purchased from Sangon company, China). Specifically, there were 10 nM M13 DNA and 100 nM of each oligonucleotide staple strand in a hybridization buffer, which contained 1 × TAE and 11 mM $MgCl_2$. This solution was mixed and subjected to the following annealing procedure: 85 °C–65 °C at a rate of 1 °C/min, and from 65 °C to 25 °C at a rate of 15 °C/min. Then, the DNA structures were purified by 1% agarose gel in 0.5 × TBE buffer with 11 mM Mg^{2+}, before being mixed with an ATP or AMP (Sigma-Aldrich) solution with the final concentration of 1 mM. The concentrations of DNA origami were determined by UV-spectrophotometer (1901, Persee).

2.2. Nanopore experiments

In this study, the SiN nanopores were fabricated on silicon nitride wafers (NJRI-001, Nanjing Rhode Nanotech Co. Ltd., China). A focused electron beam of 300 kV, 70 μA was used to form roughly a single hourglass-shaped nanopore in the center of the silicon nitride free-standing membrane by FEI Tecnai F30 TEM (Netherlands, Philips-FEI) (Fig. S1, S2 and S16). All SS-nanopore detections were performed using SS-nanopores with diameters in the range of 20–25 nm, in a 0.5 × TBE buffer with 1 M KCl and 11 mM Mg^{2+} at voltages from 100 mV to 500 mV applied by Axopatch 700B patch clamp amplifier (Axon Instruments). The DNA carrier samples were loaded with ATP by incubating with 1 mM ATP for 3 h before the translocations occurred through the SS-nanopores. The final concentration of the DNA carriers was 1 nM with excess of ATP (1 mM), based on the Kd value (6 μM) of ATP-aptamer binding (Huizenga et al., 1995).

2.3. Data analysis

The raw data, from observing the current across the single nanopore, was collected using AxoScope software. The collected data was analyzed by using the Open nanopore software suite that was developed by the Radenovic group (Granjon et al., 2012). The dwell time and the current blockade resulted from the observed translocation events (numbering in the range of 200–1000) were statistically analyzed with Matlab.

2.4. AFM characterization

The purified DNA origami ribbons were mixed with 1 mM ATP or AMP solutions. After incubation for 3 h, a KCl solution (2 M concentration) was added to create a final concentration of 1 M. Samples with or without KCl were kept under room temperature for overnight and then were pipetted onto a freshly cleaved mica surface and kept for 5 min for adsorption. Subsequent AFM measurements were carried out using a Digital Instruments Nanoscope IIIa with a liquid-cell and MultiMode head, utilizing NP-S oxide-sharpened silicon nitride probes (Vecco), under the liquid tapping mode with a scan frequency of 2–3 Hz.

2.5. Calculations of translocation events

For the SS-nanopore used in our experiment, the current signal was estimated by considering the geometrical factors, where the actual nanopore was approximately located in space relative to a cylinder structure, based on the formula by Cees Dekker (Verschueren et al., 2015a,b). Based on a concept of excluded volumes mentioned in the previous studies, a translocation model was established to calculate the current blockades caused by the DNA carriers with different surface patterns (Kowalczyk et al., 2011). In this model, three key factors were carefully taken into account: 1) the access resistance outside the nanopore; 2) the resistance in the interior volume of the nanopore; 3) the ions adsorbed on the periphery of the nanopore and on the DNA ribbon. Therefore, the conductance of an open nanopore was calculated using the following formula (Wanunu et al., 2010; Carlsen et al., 2014a, b):$G_{open} = \left(\frac{1}{\sigma d_{pore}} + \frac{4l_{pore}}{\pi\sigma {d_{pore}}^2 + 4\pi\mu_{K^+} S d_{pore}}\right)^{-1}$, where σ is the conductivity of the electrolyte, l_{pore} is the thickness of the nanopore, d_{pore} is the diameter of the nanopore, μ_{K^+} is the electrophoretic mobility of K^+, and S is the surface charge density of the nanopore walls (taken as). Here, we calculated the values of the current drop for some DNA carriers and compared the calculated values with the experimentally acquired results. The details of the calculation can be found in the support information section S16.

3. Results and discussion

3.1. Shaped DNA origami carrier design and nanopore translocation

The design of the shaped origami carrier to pass through SS-nanopore was shown in Fig. 1a. A 7249 nt M13mp18 ssDNA scaffold was hybridized with 212 staple DNA strands to form a DNA origami ribbon, which consisted of 8 parallel DNA helices. The DNA origami carrier (ribbon-1) was asymmetric with one end 9.5 nm and the other end 19.5 nm in width. In addition, a 300 nt single-stranded DNA loop overhang was designed at the narrower end to facilitate a directional

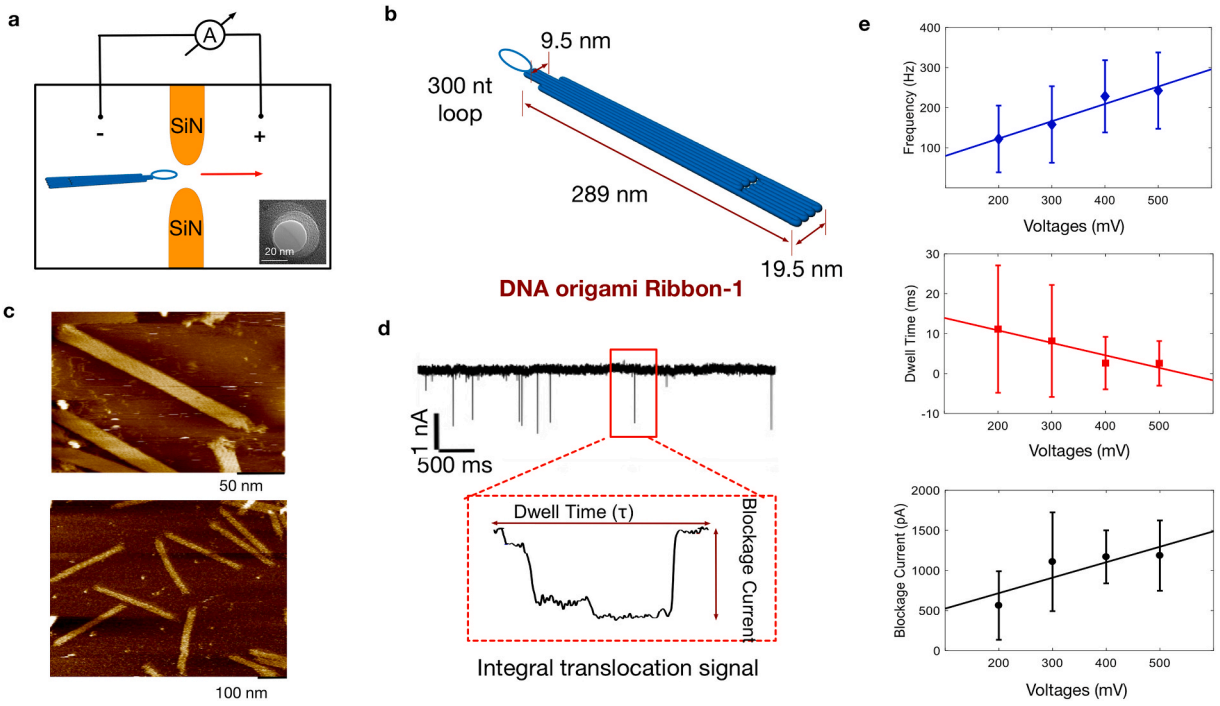

Fig. 1. DNA origami ribbon carrier translocation through SS-nanopores. (a) Schematic of the origami carrier translocation through a SS-nanopore and a TEM image of nanopore. (b) Design of the origami ribbon-1. (c) Atomic Force Microscope (AFM) characterization of ribbon-1. (d) Typical electric current traces of ribbon-1 translocation through a single SS-nanopore with 400 mV across the membrane. (e) Nanopore translocation signal variations under different voltages. Origami ribbon translocation signals recorded at 100, 200, 300, 400 and 500 mV, using 1 M KCl buffer and a 22 nm nanopore.

translocation, as it was hypothesized that the loop would enter the nanopore first and guide the DNA origami structure to go through the nanopore in a directionally controlled manner (Plesa et al., 2014) (Fig. S10). The overall length of the shaped origami ribbon (without the DNA loop overhang) was ~ 289 nm. We first examined the formation of the origami ribbons by using both AFM imaging and gel-shift assays (Fig. 1c, S5 and S6). The asymmetric design of the DNA carrier was clearly observed with AFM and its stability was confirmed in the buffers with 1M KCl (Fig. S7).

The single-molecular translocation signal of the origami carrier passing through the nanopore is shown in Fig. 1d, as a typical current trace of ribbon-1 (without surface modification). The origami carrier translocation signals were also recorded at different voltages (Fig. 1e). As the voltage increased from 100 mV to 300 mV, both the event occurrence frequency and the magnitude of the current blockage increased, while the dwell time decreased (Fig. S8). However, almost no variation tendencies of the current and dwell results can be observed from 400 mV to 500 mV. This reasons for this phenomenon may attribute to the following two aspects: 1) the tiny conformation change of origami under the different applied voltages; 2) the relative larger structures and molecular weight of origami ribbon.

3.2. *Surface aptamer modifications to influence the origami translocation*

Next, to investigate whether aptamer DNA surface modifications can influence the origami ribbon translocation, origami ribbon-2 is designed with eight decoration sites on its surface, each extended with a 27-nucleotide ATP-binding aptamer DNA (Fig. 2a). Here, the aptamers were arranged in pairs with 12 nm distance between each pair and 53 nm distance between the neighboring pairs. In the absence of ATP, the aptamer DNA stand displays a loose random coil structure. In the presence of ATP molecules, the aptamer sequence specifically binds with ATP, thus increasing the rigidity and changing the electronic charges of the aptamer strand (Fig. 2b). (Huizenga et al., 1995) In the experiment, three origami ribbon carriers were used: ribbon-1 was a control structure with no aptamer DNA modified on the surface; ribbon-2 was a ribbon with 8 aptamer DNA strands protruding from its surface in the absence of ATP molecules; ribbon-3 was a fully loaded ribbon that was completely saturated with 1 mM ATP molecules, so that all 8 aptamers displayed the rigid conformation. To investigate whether presence of free ATP molecule in the reaction solution directly influences the origami translocation, the control experiments were implemented using ribbon-1 with or without ATP (Fig. S9). The nanopore results indicate that ATP molecule present in solution has no influence on the origami carrier translocation.

In the experiments, both ribbon-1 and -3 can resulted in significant translocation results, while no such signal trace can be obtained for the ATP only sample (Fig. 2c). Signal distribution variations among the three samples can be clearly observed in the scatter plots (Fig. 2d). In the box plots of the conductance results, we found that ribbon-1 and -2 yielded lower conductance median values of 3.93 nS and 4.36 nS, and ribbon-3 resulted in a conductance median value of 6.65 nS (Fig. 2e). The results indicate ATP/aptamer binding on the ribbon surface induces significant current signal variations. Nevertheless, the dwell time median of ribbon-1, -2 and -3 had almost the same values (~0.30 ms) (Fig. 2f). This result indicates that the rigid DNA ribbon shape plays a more deterministic role in the overall passing time than the extended surface modifications.

By using Gaussian functions to analyze the nanopore current signals, it is clear to see that two Gaussian distributions can be observed as indicated by red and blue lines (Fig. 2g) (Betermier et al., 2020; Cressiot et al., 2019). The red and blue distributions may correspond to the bumping signals and translocation signals, respectively. The distributions of the red lines for ribbon-1, -2 and -3 are 1.08 ± 0.25 nA, 1.12 ± 0.31 nA and 1.76 ± 0.57 nA, respectively. For the blue lines referring to the translocation signals, the distributions of the blue lines are 2.03 ± 0.8 nA, 2.07 ± 0.31 nA and 3.38 ± 0.57 nA, respectively. Significant signal variations can be obtained by comparing the distributions of blue lines among ribbon-1, -2 and -3, than those of red lines. It can be explained as the aptamer based surface modification has more

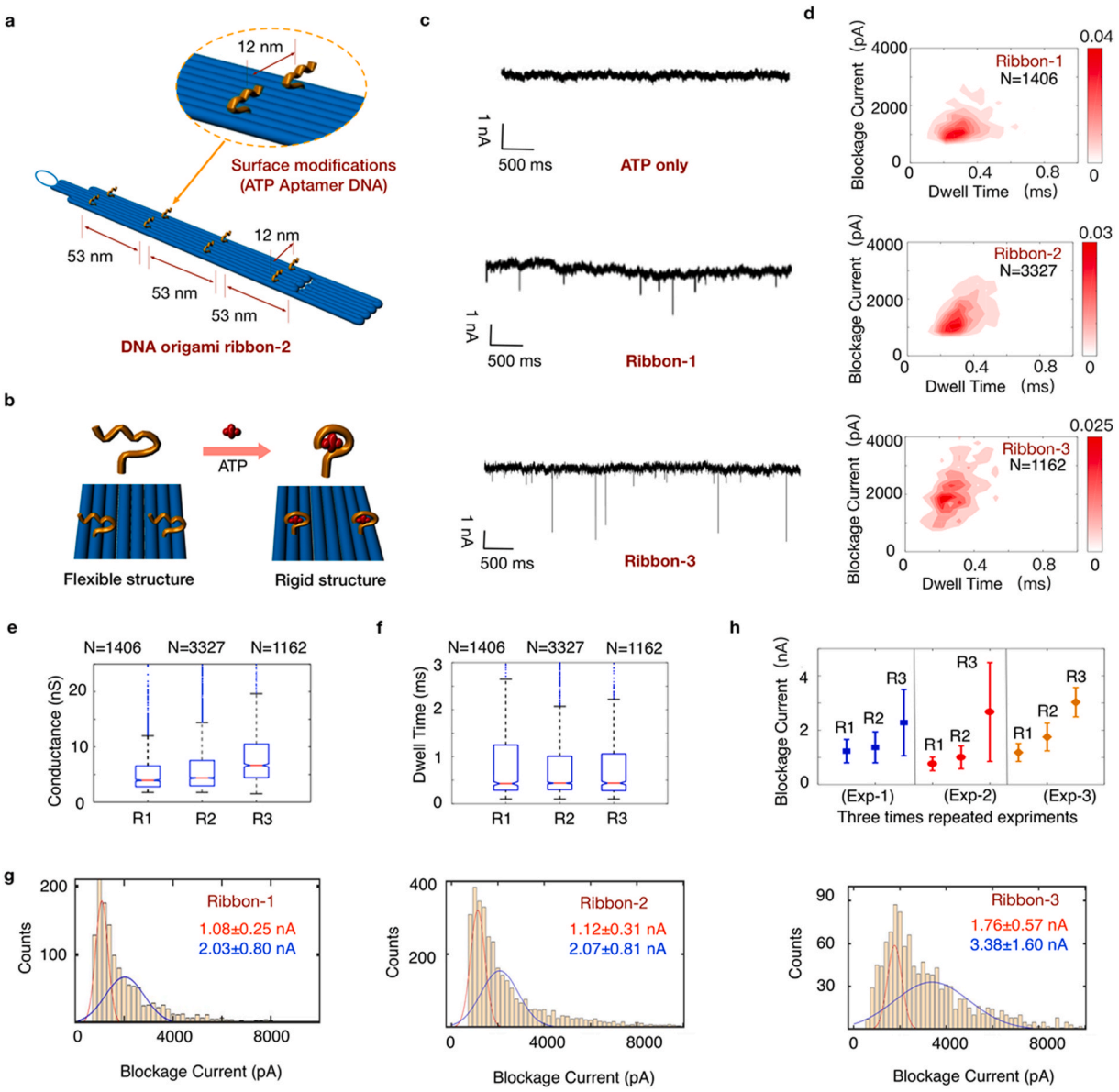

Fig. 2. Surface aptamer modifications to influence the origami carrier translocation through SS-nanopores. (a) The design of aptamer DNA modification on the surface of the carrier ribbon-2. (b) Schematic of the structural and electronic changes induced by ATP binding onto aptamer DNA. (c) Typical current traces of the translocation of ribbon-1 and -3 at 400 mV. The current trace of the sample only containing ATP without ribbon is shown on the top. (d) Scatter plots of the translocation signals corresponding to the origami carriers: ribbon-1, -2 and -3, respectively. The number of translocation events used was 1406, 3327 and 1162, respectively. The experiment was implemented in the order of ribbon-3, ribbon-2 and ribbon-1 by using the same 22 nm nanopore, and the voltage applied was 400 mV. Box plot presentation of the conductance (e) and the dwell time (f) of ribbon-1, -2 and -3 (The blue boxes denote 25th and 75th percentiles and the red lines represent the median values). (g) Using Gaussian functions to analyze the nanopore current signals. (h) Three times repeated experimental results of Exp-1, -2 and -3 using 22 nm, 21 nm and 24 nm nanopores, respectively. R1, R2 and R3 refer to ribbon-1, -2 and -3, respectively. The detection order in exp-1 is ribbon-3, -2 and -1, in exp-2 is ribbon-2, -3 and -1, in exp-3 is ribbon-2, -1 and -3. (For interpretation of the references to color in this figure legend, the reader is referred to the Web version of this article.)

influences on the translocations than those of the bumping interactions.

To confirm the repeatability of the results, the experiments were implemented in three replicates using different sample sensing orders, and the similar signal variation trends were obtained in the three repeated experiments (Fig. 2h). In addition, the nanopore analysis of DNA ribbons decorated with different numbers of aptamers, was also compared by using the experimental (Fig. S11) and theoretical (Table S1) results. Although the specific blockage current change values in the experimental and theoretical results are different, the total variation tendencies of them are similar, and that is the blockage current change values gradually growing with the aptamer numbers increasing. In addition, the directional nanopore translocation was analyzed in Fig. S10, and no significant directional control was observed. The possible reason may be that the origami ribbon translocation is a much quicker process, during which as soon as any one of the loop and ribbon ends near the nanopore, the translocation will be happened.

3.3. *The specificity of the aptamer binding induced surface modification*

To test the specificity of the aptamer binding induced surface modification, three nucleotides GTP, CTP and ATP (1 mM each) were mixed with the ribbon-4, separately (Fig. 3a). The typical current traces were obtained for ribbon-4 treated with GTP, CTP and ATP, respectively (Fig. 3b). It is clear to see that only the ribbon-4 binding with ATP can

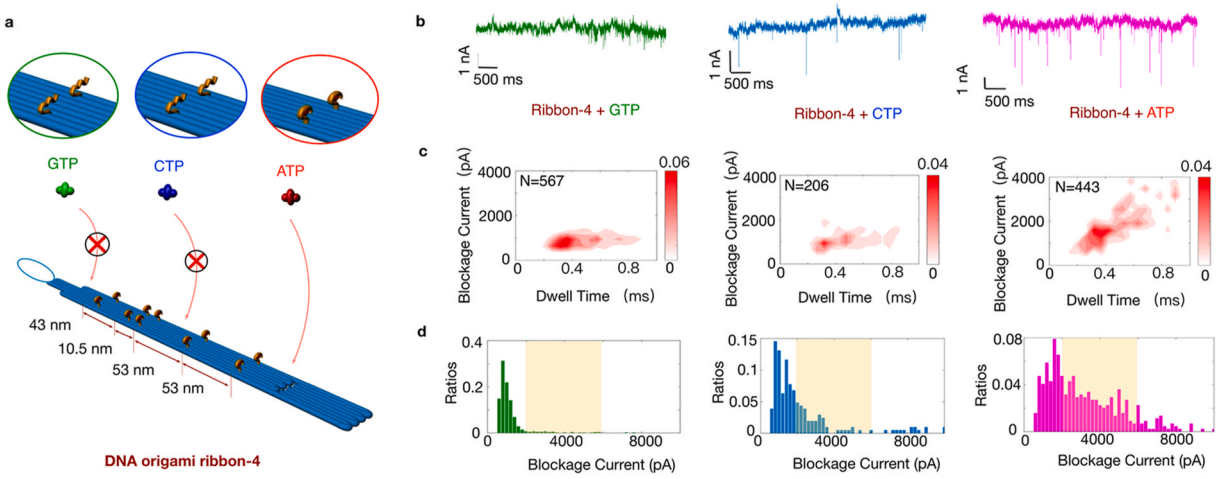

Fig. 3. The specificity of aptamer-based surface modification on origami ribbon carrier. (a) Schematic illustration of the specific binding of GTP, CTP and ATP with ribbon-4 decorated with 10 ATP aptamers. (b) Typical current trace of the translocation of ribbon-4 treated with GTP, CTP and ATP separately. (c) Scatter plots of the carrier translocation events. Three signal results were monitored in the order of ribbon-4 treated with CTP, GTP and ATP using the same 26 nm nanopore at 500 mV. The number of translocation events used was 567, 206 and 443 for the ribbon-4 treated with GTP, CTP and ATP, respectively. (d) Histograms of the current blockades show the translocation events of ribbon-4 treated with, GTP, CTP and ATP in green, blue and pink colors, respectively. (For interpretation of the references to color in this figure legend, the reader is referred to the Web version of this article.)

produce more significant target current signal variations. From the scatter plots in Fig. 3c, significant signal distribution variations can be observed among these samples, where the ATP induced signal variations have much higher blockage values. In the histograms of the current blockage (Fig. 3d), the different distribution variations are easy to discriminate, especially in the range from 2000 to 6000 pA. The mean current value of ribbon-4 treated with ATP was 2.34 ± 1.83 nA, much higher than those treated with GTP (0.88 ± 0.25 nA) or CTP (1.27 ± 0.59 nA). The results demonstrated that the ATP binding with the aptamer can induce a significant variation in the current blockage signals. That means the aptamer based surface modification is specifically induced by the aptamer DNA binding with ATP.

3.4. *Influencing the translocations by changing the spatial arrangements of the modifications*

Due to the unique addressability of DNA origami, it becomes possible to influence the origami translocations by changing the spatial arrangements of the aptamer modifications. Based on a concept of excluded ions volumes in previous studies, a translocation model was established to calculate the current blockades caused by the DNA ribbons with different surface modifications (Huizenga et al., 1995; Verschueren et al., 2015a,b). Because the ribbon nanopore translocation may induce the resistance variations within and around the nanopore, the origami ribbons with the varying locations of the surface modifications may induce different blockage current.

Here, two isomeric DNA origami ribbons were designed with the same molecular weight and different surface modification patterns: for ribbon-5, the 6 ATP/aptamer complexes were clustered together close to the narrower end of the ribbon, while for ribbon-6, the 6 aptamer/aptamer complexes were separated and spread out along the ribbon (marked by golden circles) (Fig. 4a). From the scatter plots of the translocation signals, the different signal distributions of ribbon-5 and ribbon-6 can be discriminated as indicated by the red and blue circles, respectively (Fig. 4b). An intersection point C (colored brilliant blue, with the coordinate: 0.18 ms, 3.70 nA) is obtained based on the signal overlapping distributions. In the current blockade histogram, ribbon-5 shows a smaller distribution than ribbon-6 in the high blockage range from 3.70 to 10.00 nA (Fig. 4c). And in the dwell time histogram, ribbon-5 shows a larger distribution of long dwell time than ribbon-6 in the range from 0.18 to 1.00 ms (Fig. 4d).

In Fig. 4e, by using Gaussian functions to compare the nanopore current signals, two distributions can be observed indicated by red and blue lines. Here, the red and blue distributions may correspond to the bumping signals and translocation signals, respectively. For ribbon-5, the number of the bumping interactions (red line) are more than that of the translocation interactions (blue line). However, for ribbon-6 with the linear separated aptamer arrangement, the number of the translocation interactions (blue line) become greater than that of the bumping interactions.

Here, additional experimental results were obtained from the replicate experiments using different sample sensing orders. The similar trend of the signal variations can also be obtained by comparing the mean values of current blockade and dwell time between ribbon-5 and -6 (Fig. 4f).

3.5. *Using enzyme regulated surface modification to influence the translocations*

The origami ribbon translocation was designed to be influenced by control the aptamer surface modifications via enzymatic regulation (Fig. 5a). Specifically, adenosine deaminase (ADA) can catalyze AMP to IMP resulting in a dissociation of the target molecule from the aptamer DNA (Fig. 5a) (Elbaz et al., 2009) (NOTE: AMP can bind with the same aptamer sequence of ATP with enough affinity, while IMP cannot bind as strongly as AMP). Therefore, in the presence of ADA, the ribbon-7 modified with AMP/aptamer complexes will lose the binding target and recover to the ribbon-4 without AMP induced surface modification. Moreover, similar results of the ribbon carriers binding with AMP and ATP were observed in the control experiment in Fig. S13.

To achieve the enzymatic regulation, 5 U ADA was added into ribbon-7 (a mixture containing ribbon-4 saturated with 1 mM AMP). The sample was incubated at 30 °C for 3 h to implement the enzymatic reaction (Elbaz et al., 2009). In the scatter plots in Fig. 5b, the dwell time displayed the mean value at 0.17 ± 0.08 ms, 0.25 ± 0.11 ms, and 0.17 ± 0.09 ms, for ribbon-4, ribbon-7 and recovered ribbon-4, respectively. The enzyme regulated surface modification changes are demonstrated by the almost complete recovery of the mean dwell time values. Meanwhile, the mean value of the current blockage also showed a clear recovery from 0.87 ± 0.26 nA, to 2.36 ± 0.38 nA, and back to 0.92 ± 0.31 nA for the three samples (Fig. S14).The box plots of blockage current and dwell time displayed the statistical results (Fig. 5c&d). The

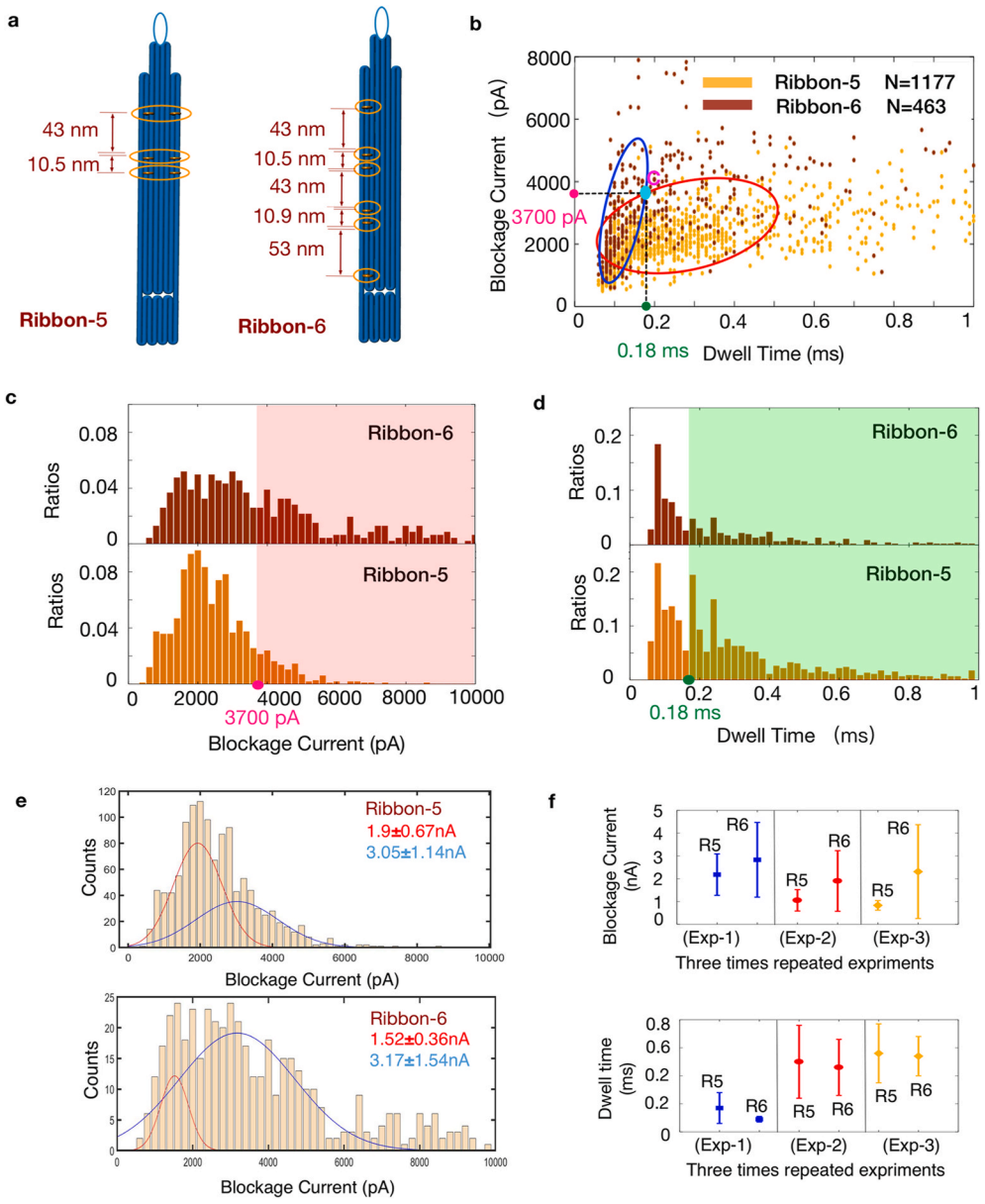

Fig. 4. Using specific spatial arrangements of the aptamer surface modifications to influence the origami translocations. (a) Schematics of origami ribbon-5 and -6 with clustered and linearly separated modification distribution of the ATP binding sites, respectively. (b) Overlapping scatter plots of DNA ribbon translocation events through a 23 nm nanopore, which was recorded at 500 mV. The experiments were monitored in the order of ribbon-6 and then ribbon-5. The number of translocation events was 1177 for ribbon-5 and 463 for ribbon-6. Histograms of current blockade (c) and dwell time (d) for ribbon-5 and -6, respectively. (e) Using Gaussian functions to analyze the nanopore current signals. (f) Three times repeated experiment results of Exp-1, -2 and -3 using 23 nm, 24 nm and 24 nm nanopores, respectively. R5 and R6 refer to ribbon-5 and -6, respectively. The detection order in exp-1 is ribbon-6 and -5, in exp-2 is ribbon-5 and -6, in exp-3 is ribbon-6 and -5.

reversibility of the nanopore signal variations demonstrated the enzyme catalyzed method can be used to control the surface modification, and subsequently regulate the origami SS-nanopore translocation.

4. Conclusions

In summary, the strategy of aptamer/target-binding modification is used to influence the special-shaped origami carrier nanopore translocations. In the SS-nanopore experiment, the specific signal variations were generated responding to the regulations of the surface modifications, induced by ATP/aptamer binding (F. S15), spatial distribution of the modifications and enzymatic reaction. The experimental results reveal that the translocation of the shaped origami ribbon across the nanopore is a complex process, susceptible to multiple factors including: origami structural shape and rigidity, electric charges, surface modification distribution and relative cross-section sizes of the nanopore and the ribbon. Meanwhile, our results also demonstrate a high sensitivity to identify small spatial and electronic changes on the shaped origami structures.

On the other hand, some aspects should be improved in the study. Firstly, in the origami translocation nanopore experiments, the manually signal analysis is complex and lack of a standard. Therefore, the recent developed deep learning based data analysis will facilitate analyzing the data in an automatic and standard manner.(Arima et al., 2018; Meyer et al., 2020; Cao et al., 2020). Secondly, the theoretical results of ribbon-2 and -3 shows a difference when compared with the experimental results. We attribute the discrepancy between the calculations and experiments to the following aspects: (1) systematic errors in the solid-state nanopore experiments, possibly arising from nanopore fabrication, measuring equipment systems and experimental operations; (2) deficiency in the calculation model, because the hypothesis used in the calculation that the solid-state nanopore is taken as a cylinder, while practically the nanopores were not of a standard cylindrical shape. Meanwhile, the simple calculation model only considered the volume excluded by aptamer based modification when DNA origami passed through the nanopore, yet didn't cover other factors, such as DNA origami seam structures, tiny conformation changes, ions adsorbed around the aptamer have not been considered. Therefore, these problems may be solved by more normalized nanopore fabrication to produce nanopores with accurate shapes and sizes. In addition, the

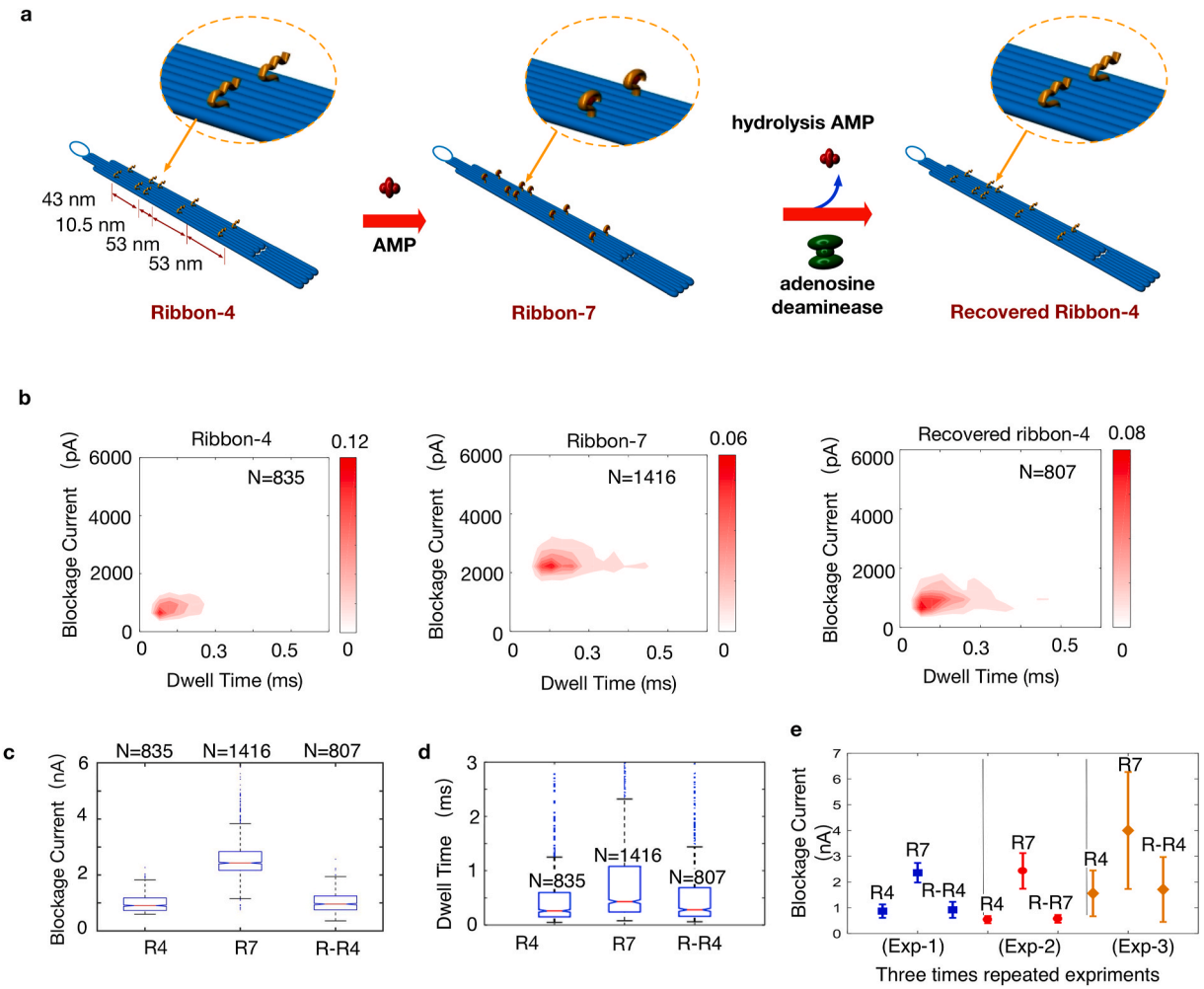

Fig. 5. Enzymatic regulation on surface modification to influence the origami carrier translocation. (a) Design of ribbon-4 with 10 aptamers on the surface. Addition of AMP to ribbon-4 forms ribbon-7. Addition of the enzyme ADA converts AMP to IMP, which dissociates from the aptamers, and the ribbon-7 is recovered back to ribbon-4. (b) Scatter plots of translocation events using a 20 nm nanopore at 500 mV. The number of translocation events used in this analysis are 835 for ribbon-4, 1416 for ribbon-7, and 807 for recovered ribbon-4. The ribbons were monitored in the order of ribbon-4, ribbon-7 and recovered ribbon-4. Box plot presentation of the blockage current (c) and dwell time (d) of ribbon-4, ribbon-7 and recovered ribbon-4. (The blue boxes denote 25th and 75th percentiles and the red lines represent the median values). (e) The results of three repeated experiments Exp-1, -2 and -3 using 20 nm, 23 nm and 26 nm nanopores, respectively. R4, R7 and R-r4 refer to ribbon-4, -7 and recovered ribbon-4, respectively. The detection order of all repeated experiments are in the order of ribbon-4, ribbon-7 and recovered ribbon-4. (For interpretation of the references to color in this figure legend, the reader is referred to the Web version of this article.)

theoretical model needs to be improved to perform more elaborated and reliable calculations.

We envision that the surface modification regulated origami nanopore translocation with fine-tunable and diverse spatial properties could potentially be applied to the areas of nanopore based molecular sensing and detection, in the near future.

CRediT authorship contribution statement

Taoli Ding: performed the experiments, Formal analysis. **Jing Yang:** Writing – original draft, Supervision. **Juan Wang:** Writing – original draft. **Victor Pan:** Writing – original draft. **Zuhong Lu:** Methodology, Supervision. **Yonggang Ke:** Methodology. **Cheng Zhang:** Methodology, Writing – original draft, Formal analysis, Supervision.

Declaration of competing interest

The authors declare that they have no known competing financial interests or personal relationships that could have appeared to influence the work reported in this paper.

Acknowledgment

We thank Prof. Yan Liu for the careful review of the manuscript, and Dr. Chun Xie for performing the simulations. This work was supported by the national key R&D program of China (2017YFE0130600 and 2016YFA0501603), National Natural Science Foundation of China (61872007, 62073133, 81871489 and 91859118), and Beijing Municipal Key R&D Project No. Z201100008320002. CAS Interdisciplinary Innovation Team (JCTD-2020-04).

Appendix A. Supplementary data

Supplementary data to this article can be found online at https://doi.org/10.1016/j.bios.2021.113658.

References

Alibakhshi, M.A., Halman, J.R., Wilson, J., Aksimentiev, A., Afonin, K.A., Wanunu, M., 2017. ACS Nano 11, 9701–9710.
Arima, A., Harlisa, I.H., Yoshida, T., Tsutsui, M., Tanaka, M., Yokota, K., Tonomura, W., Yasuda, J., Taniguchi, M., Washio, T., Okochi, M., 2018. J. Am. Chem. Soc. 140, 16834–16841.

Bell, N.A.W., Keyser, U.F., 2015. J. Am. Chem. Soc. 137, 2035–2041.
Bell, N.A.W., Keyser, U.F., 2016. Nat. Nanotechnol. 11, 645–651.
Bétermier, F., Cressiot, B., Muccio, G.D., Jarroux, N., Bacri, L., Rocca, B.M.d., Chinappi, M., Pelta, J., Tarascon, J.-M., 2020. Commun Mater 1, 59.
Bulushev, R.D., Marion, S., Petrova, E., Davis, S.J., Maerkl, S.J., Radenovic, A., 2016. Nano Lett. 16, 7882–7890.
Cao, C., Krapp, L.F., Ouahabi, A.A., König, N.F., Cirauqui, N., Radenovic, A., Lutz, J.-F., Peraro, M.D., 2020. Sci.Adv. 6, eabc2661.
Carlsen, A.T., Zahid, O.K., Ruzicka, J.A., Taylor, E.W., Hall, A.R., 2014a. Nano Lett. 14, 5488–5492.
Carlsen, A.T., Zahid, O.K., Ruzicka, J., Taylor, E.W., Hall, A.R., 2014b. ACS Nano 8, 4754–4760.
Chen, K., Kong, J., Zhu, J., Ermann, N., Predki, P., Keyser, U.F., 2019. Nano Lett. 19, 1210–1215.
Cressiot, B., Ouldali, H., Pastoriza-Gallego, M., Bacri, L., Goot, F.G.V.d., Pelta, J., 2019. ACS Sens. 4, 530–548.
Doroschak, K., Zhang, K., Queen, M., Mandyam, A., Strauss, K., Ceze, L., Nivala, J., 2020. Nat. Commun. 11, 1–8.
Elbaz, J., Moshe, M., Willner, I., 2009. Angew. Chem. 121, 3892–3895.
Giesselmann, P., Brändl, B., Raimondeau, E., Bowen, R., Rohrandt, C., Tandon, R., Kretzmer, H., Assum, G., Galonska, C., Siebert, R., Ammerpohl, O., Heron, A., Schneider, S.A., Ladewig, J., Koch, P., Schuldt, B.M., Graham, J.E., Meissner, A., Müller, F.-J., 2019. Nat. Biotechnol. 37, 1478–1481.
Guo, B., Sheng, Y., Zhou, K., Liu, Q., Liu, L., Wu, H.-C., 2018. Angew. Chem. Int. Ed. 57, 3602–3606.
Huizenga, D.E., Szostak, J.W., 1995. Biochemistry 34, 656–665.
Kawano, R., Osaki, T., Sasaki, H., Takinoue, M., Yoshizawa, S., Takeuchi, S., 2011. J. Am. Chem. Soc. 133, 8474–8477.
Kong, J., Bell, N.A.W., Keyser, U.F., 2016. Nano Lett. 16, 3557–3562.
Kovaka, S., Fan, Y., Ni, B., Timp, W., Schatz, M.C., 2021. Nat. Biotechnol. 39, 431–441.
Kowalczyk, S.W., Tuijtel, M.W., Donkers, S.P., Dekker, C., 2010. Nano Lett. 10, 1414–1420.
Kowalczyk, S.W., Grosberg, A.Y., Rabin, Y., Dekker, C., 2011. Nanotechnology 22, 315101.
Kwak, D.-K., Chae, H., Lee, M.-K., Ha, J.-H., Goyal, G., Kim, M.J., Kim, K.-B., Chi, S.-W., 2016. Angew. Chem. Int. Ed. 55, 5713–5717.
Langecker, M., Arnaut, V., Martin, T.G., List, J., Renner, S., Mayer, M., Dietz, H., Simmel, F.C., 2012. Science 338, 932–936.
Li, M.-Y., Ying, Y.-L., Li, S., Wang, Y.-Q., Wu, X.-Y., Long, Y.-T., 2020. ACS Nano 14, 12571–12578.
Lin, X., Ivanov, A.P., Edel, J.B., 2017. Chem. Sci. 8, 3905–3912.
Mcmullen, A., Haan, H.D., Tang, J.X., Stein, D., 2014. Nat. Commun. 5, 1–10.
Meyer, N., Janot, J.-M., Lepoitevin, M., Smietana, M., Vasseur, J.-J., Torrent, J., Balme, S., 2020. Biosensors 10, 140.
Plesa, C., Loo, N.V., Ketterer, P., Dietz, H., Dekker, C., 2015a. Nano Lett. 15, 732–737.
Plesa, C., Ruitenberg, J.W., Witteveen, M.J., Dekker, C., 2015b. Nano Lett. 15, 3153–3158.
Plesa, C., Verschueren, D., Pud, S., van, J., Ruitenberg, J.W., Witteveen, M.J., Jonsson, M.P., Grosberg, A.Y., Rabin, I., Dekker, C., 2016. Nanotechnology 11, 1093–1097.
Rand, A.C., Jain, M., Eizenga, J.M., Musselman-Brown, A., Olsen, H.E., Akeson, M., Paten, B., 2017. Nat. Methods 14, 411–413.
Raveendran, M., Lee, A.J., Sharma, R., Wälti, C., Actis, P., 2020. Nat. Commun. 11, 1–9.
Rivas, F., Zahid, O.K., Reesink, H.L., Peal, B.T., Nixon, A.J., Deangelis, P.L., Skardal, A., Rahbar, E., Hall, A.R., 2018. Nat. Commun. 9, 1–9.
Shasha, C., Henley, R.Y., Stoloff, D.H., Rynearson, K.D., Hermann, T., Wanunu, M., 2014. ACS Nano 8, 6425–6430.
Shim, J., Kim, Y., Humphreys, G.I., Nardulli, A.M., Kosari, F., Vasmatzis, G., Taylor, W. R., Ahlquist, D.A., Myong, S., Bashir, R., 2015. ACS Nano 9, 290–300.
Spruijt, E., Tusk, S.E., Bayley, H., 2018. Nat. Nanotechnol. 13, 739–745.
Sun, H., Yao, F., Su, Z., Kang, X.-F., 2019. Biosens. Bioelectron. 150, 111906.
Tourancheau, A., Mead, E.A., Zhang, X.-S., Fang, G., 2021. Nat. Methods 18, 491–498.
Verschueren, V.V., Jonsson, M.P., Dekker, C., 2015a. Nanotechnology 38, 234004.
Verschueren, D.V., Jonsson, M.P., Dekker, C., 2015b. Nanotechnology 26, 234004.
Wang, V., Ermann, N., Keyser, U.F., 2019. Nano Lett. 19, 5661–5666.
Wanunu, M., Dadosh, T., Ray, V., Jin, J., McReynolds, L., Drndić, M., 2010. Nat. Nanotechnol. 5, 807–814.
Wei, R., Martin, T.G., Rant, U., Dietz, H., 2012. Angew. Chem. Int. Ed. 51, 4864–4867.
Yu, J.-S., Lim, M.-C., Huynh, D.T.N, Kim, H.-J., Kim, H.-M., Kim, Y.-R., Kim, K.-B., 2015. ACS Nano 9, 5289–5298.
Zahid, O.K., Wang, F., Ruzicka, J.A., Taylor, E.W., Hall, A.R., 2016. Nano Lett. 16, 2033–2039.
Zhang, Z., Wang, X., Wei, X., Zheng, S.W., Lenhart, B.J., Xu, P., Li, J., Pan, J., Albrecht, H., Liu, C., 2021. Biosens. Bioelectron. 181, 113134.